Title	Experimental observation of temperature and magnetic-field evolution of the 4*f* states in $CeFe_2$ revealed by soft X-ray magnetic circular dichroism
Author(s)	Saito Yuji, Yasui Akira, Fuchimoto Hiroto, Nakatani Yasuhiro, Fujiwara Hidenori, Imada Shin, Narumi Yasuo, Kindo Koichi, Takahashi Minoru, Ebihara Takao, Sekiyama Akira
Citation	Physical Review B, 96(3), p.035151_1-035151_5
Text Version	Publisher's Version
URL	https://jopss.jaea.go.jp/search/servlet/search?5061038
DOI	https://doi.org/10.1103/PhysRevB.96.035151
Right	©2017 American Physical Society

Experimental observation of temperature and magnetic-field evolution of the $4f$ states in $CeFe_2$ revealed by soft x-ray magnetic circular dichroism

Y. Saitoh,[1,*] A. Yasui,[2] H. Fuchimoto,[3] Y. Nakatani,[3] H. Fujiwara,[3] S. Imada,[4] Y. Narumi,[5,†] K. Kindo,[5] M. Takahashi,[6] T. Ebihara,[6] and A. Sekiyama[3]

[1]*Materials Sciences Research Center, Japan Atomic Energy Agency (JAEA), Sayo, Hyogo 679-5148, Japan*
[2]*Japan Synchrotron Radiation Research Institute (JASRI), Sayo, Hyogo 679-5198, Japan*
[3]*Division of Materials Physics, Graduate School of Engineering Science, Osaka University, Toyonaka, Osaka 560-8531, Japan*
[4]*Department of Physical Science, Ritsumeikan University, Kusatsu, Shiga 525-8577, Japan*
[5]*The Institute for Solid State Physics, University of Tokyo, Kashiwa, Chiba 277-8581, Japan*
[6]*Department of Physics, Graduate School of Science, Shizuoka University, Shizuoka 422-8529, Japan*

(Received 24 March 2017; published 27 July 2017)

We revisit the delocalized character of the $4f$ states of $CeFe_2$ in the ferromagnetically ordered phase by x-ray magnetic circular dichroism (XMCD) in x-ray absorption spectroscopy (XAS) with improved data quality using single crystals. Surprisingly, the Ce $M_{4,5}$ XMCD spectral shape changes significantly as a function of temperature and applied magnetic field, with no concomitant changes in the spectral shape of the Ce $M_{4,5}$ XAS as well as the Fe $L_{2,3}$ XAS and XMCD. This unusual behavior is characterized by the $J = 7/2$ states in a $4f^1$ configuration mixed into the $J = 5/2$ ground state. Such extreme sensitivity of the Ce $4f$ states to the external perturbations can be related to the magnetic instability toward an antiferromagnetic phase in $CeFe_2$. Our experimental data presented here provide valuable insights into the underlying physics in strongly hybridized ferromagnetic Ce compounds.

DOI: 10.1103/PhysRevB.96.035151

I. INTRODUCTION

Intermetallic compounds containing Ce sometimes show anomalous electronic and magnetic properties associated with heavy fermions or valence-fluctuation effects [1] that have fascinated scientists for decades. In the study of these materials, pressure and magnetic field are now recognized as thermodynamic parameters that can be used to tune the electronic structure [2,3].

$CeFe_2$ orders ferromagnetically below the Curie temperature of $T_C \sim 230$ K at ambient pressure and crystallizes in a cubic $MgCu_2$-type C15 Laves phase structure [4,5]. It has been found from a number of previous investigations that the electronic structure of $CeFe_2$ is characterized by the strong hybridization between the Ce $4f$ and conduction electrons (c-f hybridization) [6–9]. The ground state of $CeFe_2$ undergoes a phase transition to an antiferromagnetic state with either chemical doping or applied pressure, which remains a subject of continuous interest and attention. Recently, Wang *et al.* have shown that the pressure and doping phase diagrams can be collapsed into a single generic phase diagram, in which the antiferromagnetic phase appears with both decreasing and increasing the lattice constant (see Fig. 2 in Ref. [10]). In addition, it is found that a Monte Carlo simulation based on a semiclassical Heisenberg model provides a good qualitative description of the phase diagram (see Fig. 6 in Ref. [10]). These findings suggest the poor correlation between the c-f hybridization and the ferromagnetic-antiferromagnetic transition, and point to the importance of the Ce-Ce exchange interaction in determining the magnetic ground state of $CeFe_2$, unlike in the case of hard magnetic materials [11].

X-ray magnetic circular dichroism (XMCD) in x-ray absorption spectroscopy (XAS) involves the excitation of core-level electrons to unoccupied states above the Fermi level, and thus offers an element- and orbital-specific proof of the magnetically polarized valence states [12]. This technique has been employed to reveal important details of both Ce and Fe contributions to the magnetism in polycrystalline $CeFe_2$ and related materials [13–17]. Here, we reinvestigate the electronic and magnetic states of $CeFe_2$ using XMCD at the Ce $M_{4,5}$ and Fe $L_{2,3}$ edges on single crystals with improved data quality with a focus on the XMCD line shape, the details of which received little attention in previous studies [14,15]. Furthermore, we go beyond the earlier studies by reporting data as a function of temperature and applied magnetic field, demonstrating that the Ce $4f$ states change significantly with these external perturbations. The present measurements provide additional information on the Ce-Ce exchange interaction between the strongly hybridized Ce $4f$ states, which is associated with the magnetic instability.

II. EXPERIMENT

High-quality $CeFe_2$ single crystals were grown by the Ce self-flux method. A superconducting quantum interface device (SQUID) magnetometer was employed for characterization of the bulk magnetization (see the Supplemental Material [18]). The XMCD experiments were performed on BL23SU at the synchrotron facility SPring-8, using the 1 Hz helicity-switching mode operation in combination with a superconducting magnet with fields up to ± 10 T [19]. XMCD spectra were derived from XAS spectra recorded for parallel (μ_+) and antiparallel (μ_-) alignment of the photon helicity

*ysaitoh@spring8.or.jp
†Present address: Center for Advanced High Magnetic Field Science, Graduate School of Science, Osaka University, Toyonaka, Osaka 560-0043, Japan.

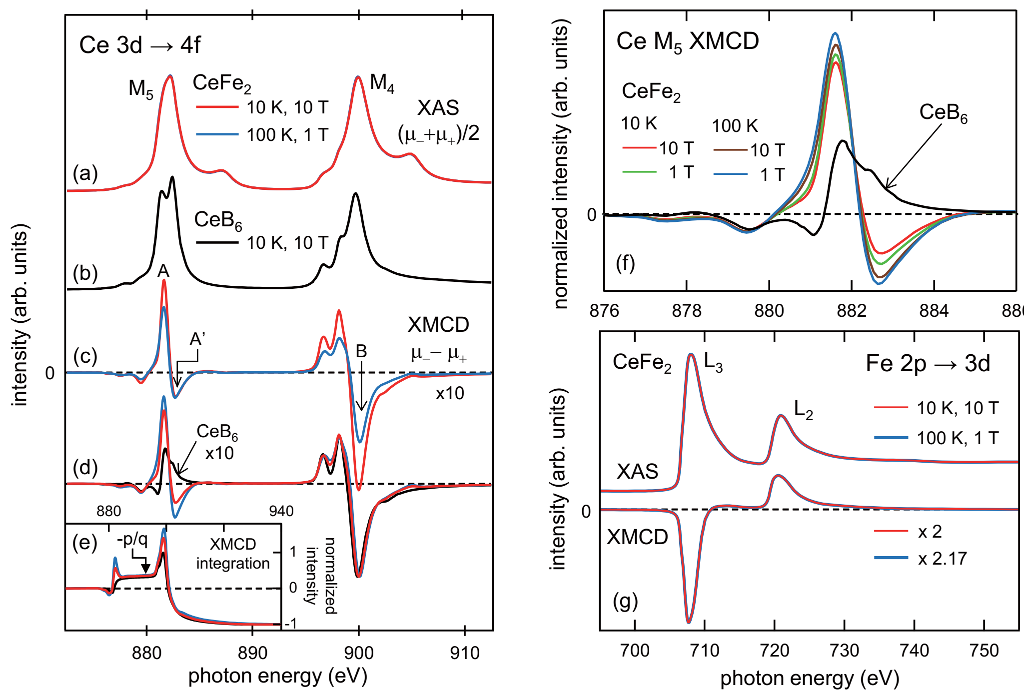

FIG. 1. Experimental results for $CeFe_2$ measured at $T = 10$ K with $H = 10$ T (red curves) and at 100 K with 1 T (blue curves) compared with those for CeB_6 at 10 K with 10 T (black curves). (a),(b) Ce $M_{4,5}$ XAS and (c),(d) XMCD spectra. (d) The spectra are normalized to the maximum Ce M_4 peak intensity. (e) Normalized XMCD integration curves. (f) Ce M_5 XMCD in (d) together with those obtained at 10 K with 1 T and 100 K with 10 T, all normalized to the maximum Ce M_4 peak intensity. (g) Fe $L_{2,3}$ XAS and XMCD spectra of $CeFe_2$.

with the applied magnetic field collinear with the photon beam. All the spectra were obtained in total electron yield mode by monitoring the total sample photocurrent normalized to the incoming radiation flux with an energy resolution of 0.1 eV or better. In order to minimize experimental artifacts arising from system errors, each XMCD spectrum was measured for opposite orientations of the applied magnetic field and the resulting spectra were averaged. The single-crystal samples were cleaved in an ultrahigh vacuum to expose clean (111) surfaces and cooled with a flowing He cryostat. A CeB_6 (001) single crystal was also measured as a reference with a nearly Ce^{3+} valence state [20].

III. RESULTS AND DISCUSSION

In Figs. 1(a)–1(d), we show the XAS, $(\mu_- + \mu_+)/2$, and XMCD, $\mu_- - \mu_+$, spectra measured across the Ce $M_{4,5}$ edges for $CeFe_2$ at a temperature of $T = 10$ K with an applied field of $H = 10$ T and at 100 K with 1 T, together with those for the reference compound CeB_6 at 10 K with 10 T. The XAS and XMCD spectra of CeB_6 in Figs. 1(b) and 1(d) exhibit the characteristic structure of a Ce^{3+} f^1 configuration with a total angular momentum $J = 5/2$ due to electric-dipole transitions from $3d^{10}4f^1$ ground state to $3d^9 4f^2$ final states [21,22]. The differences in the XAS and XMCD spectral shapes between $CeFe_2$ and CeB_6 arise from the c-f hybridization as described below.

Surprisingly, the XMCD curves for $CeFe_2$ shown in Fig. 1(c) display a nonuniform change in the spectral shape without any appreciable change in the corresponding XAS curves, as shown in Fig. 1(a). It should be noted that no phase transition has been detected in between the two experimental conditions and little volume expansion was reported inside the magnetically ordered state in $H = 0$ by Kennedy *et al.* [23]. In addition, no impurity peaks are detected by hard x-ray photoemission spectroscopy on our samples, as shown in Fig. S2 in the Supplemental Material [18]. To facilitate the comparison of the XMCD spectral shapes for $CeFe_2$, the XMCD data normalized at the maximum XMCD amplitude at the Ce M_4 edge are shown in Fig. 1(d), together with that of CeB_6. Clear differences in the spectral shape are seen at the M_5 edge. Figure 1(e) shows the energy-integration curves of these XMCD spectra normalized to their values at 940 eV, which provide additional information on the magnetic moments as described below. Figure 1(f) summarizes the Ce M_5 edge XMCD curves in Fig. 1(d) along with those obtained at 10 K with 1 T and at 100 K with 10 T on $CeFe_2$, all of which are normalized to the Ce M_4 XMCD peak. It can be seen that the XMCD features for $CeFe_2$ has a systematic dependence on H and T.

By contrast, at the Fe $L_{2,3}$ edges, the XAS and XMCD in $CeFe_2$ both exhibit no change in the spectral shapes between the data at the same conditions, as shown in Fig. 1(g). This is the usual behavior and can be commonly observed in most materials.

In Fig. 2(a), we show the dependence of the Fe L_3 XMCD peak intensity on H measured at 10 and 100 K. Since the Fe XAS and XMCD spectral shapes are independent of H and T, these curves provide conventional element-specific magnetization profiles [24]. The inset shows the T dependence of the SQUID bulk-magnetization M measured at 1 and 7 T along the [111] direction. It can be seen that the Fe XMCD signal, hence the magnitude of the Fe $3d$ moment,

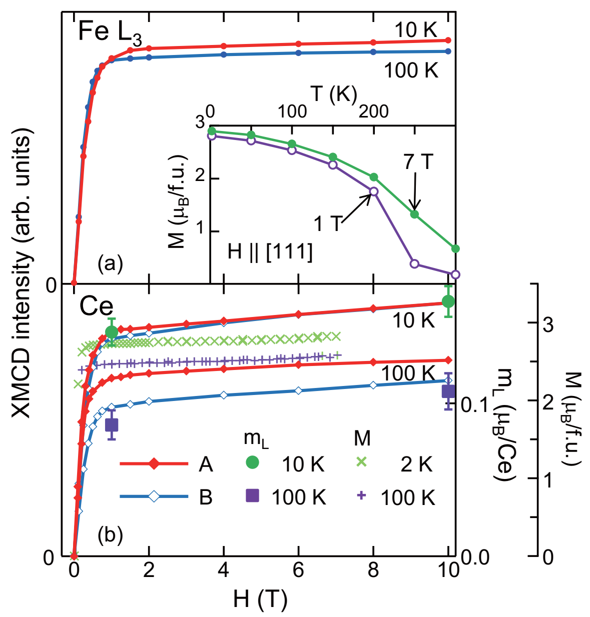

FIG. 2. (a) Fe L_3 XMCD peak intensity as a function of applied magnetic field at 10 and 100 K. Inset: temperature dependence of the bulk magnetization $M(T)$ under 1 and 7 T. (b) Field scans of the Ce $M_{4,5}$ XMCD signals at peak A and peak B as marked in Fig. 1(c) for 10 and 100 K normalized at 10 K with 10 T along with the XMCD-derived Ce $4f$ orbital moments and $M(H)$ data at 2 and 100 K.

scales proportionally to M. This is the case for the Ce $5d$ moment, but is coupled antiparallel to the Fe $3d$ moment [13]. Sum-rule analysis [25–27] with a calculated number of Fe $3d$ electrons of 6.18 [7] for the experimental Fe spectra at 10 K with 10 T yields a total moment of $m_{\text{total}} = m_L + m_S = -\langle L_z\rangle - 2\langle S_z\rangle = 1.6\mu_B$/Fe, with an orbital-to-spin magnetic moment ratio of $m_L/m_S = \langle L_z\rangle/2\langle S_z\rangle = 0.05$ for the Fe $3d$ state. The systematic error is expected to be $\pm 5\%$ or less. These values are within the range of the results of previous band structure calculations [5,7,28,29].

Similar isothermal measurements at the Ce $M_{4,5}$ XMCD peaks marked A and B in Fig. 1(c) are shown in Fig. 2(b) by solid lines. Here the data have been normalized to the intensity at 10 K with 10 T. Both of the peaks show a ferromagnetic response, but with different dependences on H and T, reflecting the unusual behavior of the Ce XMCD shape. In addition, the T dependence for the two peaks differs significantly. It should be noted here that the intensity of the negative XMCD peak marked A′ in Fig. 1(c) remains almost constant under the measured four conditions given in Fig. 1(f).

In principle, the m_L and m_S contributions to the Ce $4f$ moment can be investigated independently by applying the corrected XMCD sum rules [25,26,30] given by

$$\langle L_z\rangle = \frac{q(14-n_f)}{r}, \tag{1}$$

$$\frac{\langle L_z\rangle}{\langle S_z\rangle} = \frac{4C}{5p/q-3}\left(1+\frac{\langle T_z\rangle}{\langle S_z\rangle}\right), \tag{2}$$

where p (q) is the integral of the XMCD signal over the M_5 edge ($M_{4,5}$ edges), r is the integral of the polarization-averaged

TABLE I. Values of m_L/m_S, m_S, and m_{total} obtained from the Ce $M_{4,5}$ XMCD at 10 K with 10 T through application of the sum rules as possible upper and lower bounds of m_{total}.

C	$\langle T_z\rangle/\langle S_z\rangle$	m_L/m_S	m_S (μ_B/Ce)	m_{total} (μ_B/Ce)
1.6	8/5	−4.0	−0.042	0.13
1	0	−0.43	−0.39	−0.22

XAS intensity over the $M_{4,5}$ edges, and n_f is the Ce $4f$ occupation number. C is a correction factor due to the large jj mixing between $3d_{5/2}$ and $3d_{3/2}$ core levels. $\langle T_z\rangle$ is the magnetic dipole term. However, the application of the second sum rule is complicated by possibly large contributions of C and $\langle T_z\rangle$. These terms are difficult to measure experimentally. The theoretical XMCD spectrum for a Ce^{3+} ion ($J = 5/2$ ground state) with $m_L/m_S = -4$ and $\langle T_z\rangle/\langle S_z\rangle = 8/5$ are characterized by $C = 1.6$ [30], while the $C(\langle T_z\rangle/\langle S_z\rangle)$ value is thought to approach 1 (0) with increasing c-f hybridization [15]. This leads to large uncertainties even in the sign of m_{total} as shown in Table I, where the results with $n_f = 0.7$ [7,31] for the experimental spectra at 10 K with 10 T are listed. The uncertainty in n_f is not important as long as $n_f \ll 14$. Previous calculations [5,7,28,29] yield $m_{\text{total}} = -0.54$–$-0.26\mu_B$/Ce with $m_L/m_S = -0.53$–-0.35, which are in line with those derived from the sum rules using $C = 1$ and $\langle T_z\rangle/\langle S_z\rangle = 0$. Note here that our experimental findings shown in Fig. 1(e) indicate that the observed changes in the XMCD shape are accompanied by no clear change in the p/q ratio with a similar value identical to what is expected for a localized Ce^{3+} ion ($p/q = -0.33$) [30] within the experimental uncertainty. Therefore, the m_L/m_S value for $C = 1.6$ and $\langle T_z\rangle/\langle S_z\rangle = 8/5$ in Table I retains the free-ion value of -4.

In Fig. 2(b), we have plotted the m_L values obtained from the measured spectra using Eq. (2) with $n_f = 0.7$ for the scale on the left axis. This figure illustrates the proportionality between the Ce M_4 XMCD peak intensity and m_L with a T dependence different from that of the Fe $3d$ moment. A similar behavior is known to be responsible for the compensation temperature in ferrimagnetic $3d$-$4f$ compounds, in which the temperature dependence of the $4f$ magnetization is largely determined by the exchange field from the $3d$ sublattice [4,32,33].

Our XAS and XMCD results on $CeFe_2$ at 10 K with 1 T are basically similar in shape to those observed previously from polycrystalline $CeFe_2$ [15], except that the fine structures in the Ce $M_{4,5}$ XMCD data are better resolved in the present study. It has been shown by Antonov *et al.* that calculations based on band structure considerations are useful in the description of the previous experimental XAS and XMCD data for the Fe $L_{2,3}$ edges, but not for the Ce $M_{4,5}$ edges in terms of the satellite structure in XAS and the fine structure in XMCD. [5] It has also been shown, using the single-impurity Anderson model, that the c-f hybridization give rise to an admixture of the $4f^0$ and $4f^1$ with $J = 7/2$ configurations into the $4f^1$ with $J = 5/2$ ground state, which results in the appearance of the XAS satellite, the smearing of the multiplet-split main peaks in the XAS spectra, and the change in XMCD line shape [34,35].

It is clear that a detailed theoretical analysis of the spectral shapes and the magnitude of the Ce XMCD signals is

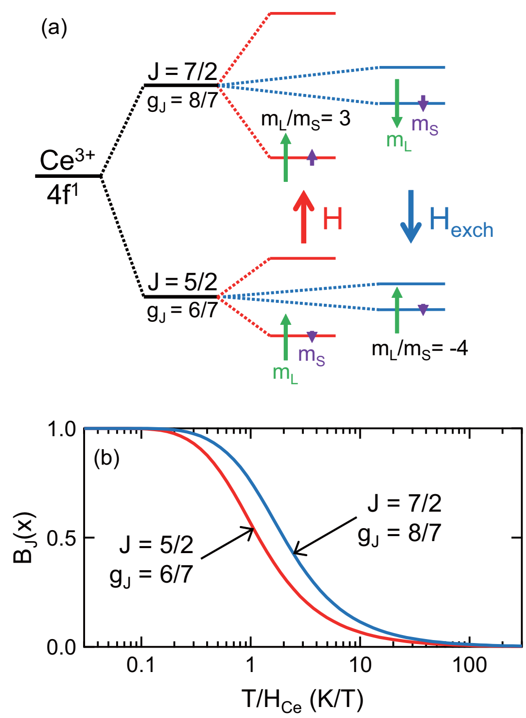

FIG. 3. (a) Schematic illustration of the different effects of applied (H) and exchange ($H_{\rm exch}$) fields on the magnetic moments originated from a Ce^{3+} $4f^1$ configuration. The spin (m_S) and orbital (m_L) moments are coupled antiparallel and parallel to each other within the $J = 5/2$ and $7/2$ states, respectively, following Hund's rule. The total moments, $m_{\rm total} = m_S + m_L$, of the $J = 5/2$ and $7/2$ states are magnetically aligned parallel by H, while aligned antiparallel by $H_{\rm exch}$. (b) Brillouin functions for $J = 5/2$ and $J = 7/2$ plotted as a function of $T/H_{\rm Ce}$.

required for a full description of the experimental results. However, our findings in Fig. 1(e) indicate that the magnetic contribution from the $J = 7/2$ component relative to the $J = 5/2$ component increases with increasing (decreasing) T (H), whereas in Fig. 1(a), n_f remains essentially unchanged. Such behavior can be roughly understood by considering the difference between the basic magnetic properties of the $J = 5/2$ and $7/2$ states with different Landé-g_J factors of $6/7(<1)$ and $8/7(>1)$, respectively. In a simplified single-ion model, the effective local magnetic field at the Ce site is given by [4,36,37]

$$H_{\rm Ce} = H + H_{\rm m} = H + \frac{2(g_J - 1)}{g_J} H_{\rm exch}, \qquad (3)$$

where $H_{\rm m}$ is the molecular field determined by the values of g_J and the exchange field $H_{\rm exch}$ acting only on the $4f$ spins. The $H_{\rm exch}$ value at low temperature for $CeFe_2$ has been estimated to be approximately -90 T [37], giving $H_{\rm m} \sim 30$ and -22.5 T for the g_J values of 6/7 and 8/7, respectively. Specifically, H used to align the magnetization of the sample and $H_{\rm exch}$ have opposite directions, as schematically shown in Fig. 3(a). This is because the Fe $3d$ and Ce $4f$ spins are coupled antiparallel as verified by the sum-rule analysis given in Table I. Such antiparallel spin coupling is typical of $3d$-$4f$ magnets [4,11,37]. Consequently, H ($H_{\rm exch}$) magnetically aligns the $J = 5/2$ and $7/2$ states parallel (antiparallel), as shown in Fig. 3(a). In other words, H ($H_{\rm exch}$) aligns the direction of $m_{\rm total}$ (m_S) of these two states. Such magnetic interactions can account for the observed H dependence in the Ce XMCD, since the application of H results in some cancellation of the $J = 7/2$ contribution.

In this single-ion model, the magnetization per Ce ion is approximated by $m = m_0 B_J(x)$ with $J = 5/2$, where $m_0 = g_J J \mu_{\rm B}$, $B_J(x)$ is the Brillouin function, and $x = m_0 H_{\rm Ce}/k_{\rm B}T$ with the Boltzmann constant $k_{\rm B}$. In Fig. 3(b), we plot $B_{5/2}(x)$ as a function of $T/H_{\rm Ce}$ and compare it with $B_{7/2}(x)$ for a virtual $J = 7/2$ ground state, illustrating a distinct difference in magnetic behavior between the $J = 5/2$ and $7/2$ states. Our simple picture also provides a qualitative description of the T-dependent XMCD results that can be interpreted as being due to the smaller dependence of the $J = 7/2$ contribution than that of the $J = 5/2$ contribution on T for a nearly constant value of $H_{\rm exch}$.

The Monte Carlo simulation noted in Sec. I illustrates that the magnetic ordering temperature is controlled by J_1 and the ferromagnetic (FM) to antiferromagnetic (AF) phase boundary is controlled by J_3/J_2, where J_1, J_2, and J_3 are the Fe-Ce, Fe-Fe, and Ce-Ce exchange strengths, respectively. Note that the FM-AF boundary is temperature independent within this simulation, in contrast to the experimental FM-AF boundary. In this simulation, the spins are treated as classical Ising spins with no T dependence. Our observation of the unusual T evolution of the Ce XMCD at 1 T should be associated with the T dependence of J_3, on which the $J = 7/2$ contribution in the ground state caused by the c-f hybridization can lead to additional effects. This should be useful in the development of a theory beyond the simple model by replacing the Ising $4f$ spins with the strongly hybridized $4f$ spins.

Finally, it should be point out that as with many rare-earth compounds [20], there is a surface Ce valence shift toward Ce^{3+} in $CeFe_2$ [6,7,31], the effect of which is not included in the above discussion. This is because very little has been reported on the surface magnetic properties of $CeFe_2$ and almost all the ferromagnetic Ce compounds with nearly localized $4f$ moments have low-$T_{\rm C}$ values [3]. However, we cannot rule out the possibility of a ferromagnetic order of the surface Ce moments of $CeFe_2$ with a $T_{\rm C}$ of above 100 K. Since a Ce^{3+} ion can have magnetic moment up to 2.14 $\mu_{\rm B}$, the surface Ce contribution to the XMCD using the total electron yield method is not always negligible. This remains as an open question.

IV. CONCLUSION

To conclude, by means of high-quality XMCD, we demonstrated that the $4f$ states in $CeFe_2$ change appreciably with temperature and magnetic field in the ferromagnetically ordered phase. The Fe $3d$ moment is simply proportional to the bulk magnetization. The remarkable behavior of the Ce XMCD is interpreted as arising from a mixed ground state of the Ce atoms involving the $J = 5/2$ and $7/2$ states of a $4f^1$ configuration caused by c-f hybridization, in which the exchange field produced by the Fe sublattice plays a key role. Furthermore, the observed evolution as a function of temperature is probably reflected in the Ce-Ce exchange interaction, which is associated with the instability toward an antiferromagnetic phase in $CeFe_2$ on the basis of a theoretical simulation. Our results will help to guide and inform future investigations.

ACKNOWLEDGMENTS

The authors acknowledge Y. Takeda, K. Fukushima, C. Hatakeyama, T. Mori, and T. Yamaguchi for their help with the XMCD experiments. The XMCD measurements were performed under the approval of BL23SU at SPring-8 (Proposals No. 2011B3834, No. 2012A3834, and No. 2012B3834). This work was financially supported by Grants-in-Aid for Scientific Research on Innovative Areas (Grants No. JP20102003 and No. JP16H01074), a Grant-in-Aid for Young Scientists (Grant No. JP23740240), and a Grant-in-Aid for Scientific Research (Grant No. JP16H04014) from the Ministry of Education, Culture, Sports, Science and Technology, Japan.

[1] For a review, see P. Coleman, in *Handbook of Magnetism and Advanced Magnetic Materials*, edited by H. Kronmüller and S. Parkin (Wiley, New York, 2007), and references therein.
[2] Q. Si and F. Steglich, Science **329**, 1161 (2010).
[3] M. Brando, D. Belitz, F. M. Grosche, and T. R. Kirkpatrick, Rev. Mod. Phys. **88**, 025006 (2016).
[4] J. J. M. Franse and R. J. Radwanski, in *Handbook of Magnetic Materials*, edited by K. H. J. Buschow (North-Holland, Amsterdam, 1993), Vol. 7, p. 307.
[5] V. N. Antonov, D. A. Kukusta, and A. N. Yaresko, Phys. Rev. B **78**, 094401 (2008).
[6] L. Braicovich, N. B. Brookes, C. Dallera, M. Salvietti, and G. L. Olcese, Phys. Rev. B **56**, 15047 (1997).
[7] T. Konishi, K. Morikawa, K. Kobayashi, T. Mizokawa, A. Fujimori, K. Mamiya, F. Iga, H. Kawanaka, Y. Nishihara, A. Delin, and O. Eriksson, Phys. Rev. B **62**, 14304 (2000).
[8] R.-J. Jung, H.-D. Kim, B.-H. Choi, S.-J. Oh, E.-J. Cho, T. Iwasaki, A. Sekiyama, S. Imada, S. Suga, and J.-G. Park, J. Electron Spectrosc. Relat. Phenom. **114**, 693 (2001).
[9] A. Kotani, K. O. Kvashnina, P. Glatzel, J. C. Parlebas, and G. Schmerber, Phys. Rev. Lett. **108**, 036403 (2012).
[10] J. Wang, Y. Feng, R. Jaramillo, J. van Wezel, P. C. Canfield, and T. F. Rosenbaum, Phys. Rev. B **86**, 014422 (2012).
[11] M. D. Kuz'min, Y. Skourski, D. Eckert, M. Richter, K.-H. Müller, K. P. Skokov, and I. S. Tereshina, Phys. Rev. B **70**, 172412 (2004).
[12] G. van der Laan and A. I. Figueroa, Coord. Chem. Rev. **277**, 95 (2014).
[13] C. Giorgetti, S. Pizzini, E. Dartyge, A. Fontaine, F. Baudelet, C. Brouder, Ph. Bauer, G. Krill, S. Miraglia, D. Fruchart, and J. P. Kappler, Phys. Rev. B **48**, 12732 (1993).
[14] J. Ph. Schillé, F. Bertran, M. Finazzi, Ch. Brouder, J. P. Kappler, and G. Krill, Phys. Rev. B **50**, 2985 (1994).
[15] A. Delobbe, A.-M. Dias, M. Finazzi, L. Stichauer, J.-P. Kappler, and G. Krill, Europhys. Lett. **43**, 320 (1998).
[16] J. Chaboy, C. Piquer, L. M. García, F. Bartolomé, H. Wada, H. Maruyama, and N. Kawamura, Phys. Rev. B **62**, 468 (2000).
[17] N. Jaouen, S. G. Chiuzbăian, C. F. Hague, R. Delaunay, C. Baumier, J. Luning, A. Rogalev, G. Schmerber, and J.-P. Kappler, Phys. Rev. B **81**, 180404(R) (2010).
[18] See Supplemental Material at http://link.aps.org/supplemental/10.1103/PhysRevB.96.035151 doi for details of the sample characterization.
[19] Y. Saitoh, Y. Fukuda, Y. Takeda, H. Yamagami, S. Takahashi, Y. Asano, T. Hara, K. Shirasawa, M. Takeuchi, T. Tanaka, and H. Kitamura, J. Synchrotron Radiat. **19**, 388 (2012).
[20] S. Imada, A. Sekiyama, and S. Suga, J. Phys.: Condens. Matter **19**, 125204 (2007).
[21] B. T. Thole, G. van der Laan, J. C. Fuggle, G. A. Sawatzky, R. C. Karnatak, and J.-M. Esteva, Phys. Rev. B **32**, 5107 (1985).
[22] Y. Saitoh, H. Fujiwara, T. Yamaguchi, Y. Nakatani, T. Mori, H. Fuchimoto, T. Kiss, A. Yasui, J. Miyawaki, S. Imada, H. Yamagami, T. Ebihara, and A. Sekiyama, J. Phys. Soc. Jpn. **85**, 114713 (2016).
[23] S. J. Kennedy and B. R. Coles, J. Phys.: Condens. Matter **2**, 1213 (1990).
[24] C. T. Chen, Y. U. Idzerda, H.-J. Lin, G. Meigs, A. Chaiken, G. A. Prinz, and G. H. Ho, Phys. Rev. B **48**, 642 (1993).
[25] B. T. Thole, P. Carra, F. Sette, and G. van der Laan, Phys. Rev. Lett. **68**, 1943 (1992).
[26] P. Carra, B. T. Thole, M. Altarelli, and X. Wang, Phys. Rev. Lett. **70**, 694 (1993).
[27] C. T. Chen, Y. U. Idzerda, H. J. Lin, N. V. Smith, G. Meigs, E. Chaban, G. H. Ho, E. Pellegrin, and F. Sette, Phys. Rev. Lett. **75**, 152 (1995).
[28] O. Eriksson, L. Nordstrom, M. S. S. Brooks, and B. Johansson, Phys. Rev. Lett. **60**, 2523 (1988).
[29] J. Trygg, J. M. Wills, B. Johansson, and O. Eriksson, Phys. Rev. B **50**, 4200 (1994).
[30] Y. Teramura, A. Tanaka, B. T. Thole, and T. Jo, J. Phys. Soc. Jpn. **65**, 3056 (1996).
[31] K. Asakura, K. Fukui, H. Ogasawara, I. Harada, J. C. Parlebas, and A. Kotani, J. Phys. Soc. Jpn. **73**, 2008 (2004).
[32] W. P. Wolf, Rep. Prog. Phys. **24**, 212 (1961).
[33] A. E. Clark and E. Callen, J. Appl. Phys. **39**, 5972 (1968).
[34] T. Jo and S. Imada, J. Phys. Soc. Jpn. **59**, 1421 (1990).
[35] M. Finazzi, F. M. F. de Groot, A.-M. Dias, B. Kierren, F. Bertran, Ph. Sainctavit, J.-P. Kappler, O. Schulte, W. Felsch, and G. Krill, Phys. Rev. Lett. **75**, 4654 (1995).
[36] W. P. Wolf and J. H. Van Vleck, Phys. Rev. **118**, 1490 (1960).
[37] R. G. Radwanski, Z. Phys. B **65**, 65 (1986).